Models for Vortex-Induced Vibration of Cylinders Based on Measured Forces

Robert D. Blevins
Goodrich,
850 Lagoon Drive,
Chula Vista, CA 91910

This paper develops experimentally based nonlinear models for the vortex shedding forces on oscillating cylinders. The lift in-phase and out-of-phase with cylinder motion and mean drag are determined from experiments with cylinder amplitudes from 0.05 cm to 1.5 cm, and reduced velocities between 2 and 12. The results are reduced to a uniform grid, tabulated, and applied to prediction of resonant, nonresonant, and time history vortex-induced vibration. The results are reduced to a uniform grid, tabulated, and applied to prediction of resonant, nonresonant and time history vortex-induced vibration.
[DOI: 10.1115/1.3222906]

1 Introduction

It is well known that cylinders in steady cross flow shed vortices that create the periodic vortex street, as shown in Fig. 1 [1], and induce vibration of elastic cylinders such as pipelines, thermowells, and stacks [2–5]. However, accurate prediction of vortex-induced vibration has proved difficult, owing to nonlinear fluid forces and feedback between the cylinder and the fluid flow [5–11]. This paper develops experimentally based models for the forces imposed by the periodic vortex shedding on oscillating cylinders. These are applied to prediction of vortex-induced vibration of elastic structures in fluid flow.

Figure 2 presents existing measurements for maximum amplitude of lightly damped elastic cylinders (top), Strouhal number (middle), and drag coefficient of stationary cylinders (bottom) as functions of Reynolds number $\mathrm{Re}=UD/\nu$, where ν is the fluid kinematic viscosity [6,12–22]. The Strouhal number (St) is the dimensionless proportionality constant between the vortex shedding frequency (f_s) from a stationary cylinder in Hz and the freestream velocity (U) divided by the cylinder diameter (D) in the same unit system.

$$f_s = \mathrm{St}U/D \tag{1}$$

It is also the frequency of oscillating lift forces on a stationary cylinder. The mean drag coefficient is defined as

$$C_{Do} = F_D/[(1/2)\rho U^2 DL] \tag{2}$$

where F_D is the mean drag force, which is the force in the direction of freestream flow on a cylinder length L in a cross flow averaged over many vortex shedding cycles, and ρ is the fluid density.

Below about $\mathrm{Re}=5\times10^5$, the Strouhal number and drag coefficient for a stationary cylinder are functions of the Reynolds number. Above about $\mathrm{Re}=10^5$ they are also functions of the cylinder surface roughness k. Above 5×10^5, they are nearly independent of Reynolds number for rough surface cylinders [14,21]. Empirical fits have been made to the Strouhal number data for rough surface stationary cylinders in Fig. 2.

$$\mathrm{St} = \begin{cases} 0.22(1-22/\mathrm{Re}), & 45 \le \mathrm{Re} < 1300 \\ 0.213 - 0.0248(\log_{10}\mathrm{Re}/1300)^2 + 0.0095(\log_{10}\mathrm{Re}/1300)^3 & \\ \qquad\qquad 1300 \le \mathrm{Re} < 5\times10^5 & \\ 0.22, \quad 5\times10^5 < \mathrm{Re} < 10^7 & \end{cases} \tag{3}$$

The first and last expression are based on Refs. [14,21,22]. The middle expression is a fit to the data of Norberg [13] between $1300<\mathrm{Re}<5\times10^5$. Also see Refs. [7,23].

2 Models for Vortex-Induced Forces on Cylinders

Vortex-induced fluid forces on oscillating cylinders are functions of the cylinder motion. Cylinder vibration, at or near the shedding frequency with amplitude above about a few percent of cylinder diameter, increases the strength of the shed vortices and the spanwise correlation of the wake, and shifts the vortex shedding frequency from the stationary cylinder shedding frequency (Eq. (1)) toward the cylinder vibration frequency [8–11,24–27], which is called lock-in, entrainment, or synchronization. As a result lift measured on a stationary cylinder is not generally a reliable predictor of vortex-induced cylinder motion.

Three models for the time dependent fluid dynamic forces per unit span on a cylinder in the direction of displacement $y(t)$ are (a) the oscillating drag model for oscillations in still fluid, (b) lift coefficient model with forcing at the stationary shedding frequency f_s (Eq. (1)), and (c) the two parameter self-excitation model of Hartlen and Currie [28] and Sarpkaya [29] with in-phase and out-of-phase forces at cylinder oscillation frequency f.

$$F_y = -(1/2)\rho|\dot{y}|\dot{y}DC_D - \rho(\pi/4)D^2C_a\ddot{y}, \quad (U=0) \tag{4a}$$

$$F_y = (1/2)\rho U^2 DC_L \sin(2\pi f_s t + \varphi) \tag{4b}$$

$$F_y = (1/2)\rho U^2 DC_{mv}\sin(2\pi ft) - (1/2)\rho U^2 DC_{dv}\cos(2\pi ft) \tag{4c}$$

The over dot ($\bullet$) denotes differentiation with respect to time. If the cylinder motion is harmonic in time with amplitude A_y and frequency f in Hz, that is

Contributed by the Fluids Engineering Division of ASME for publication in the JOURNAL OF FLUIDS ENGINEERING. Manuscript received May 20, 2008; final manuscript received July 26, 2009; published online September 30, 2009. Assoc. Editor: Joseph Katz.

Fig. 1 Vortex street behind a stationary cylinder [1]

$$y(t) = A_y \sin(2\pi ft), \quad \frac{dy}{dt} = A_y(2\pi f)\cos(2\pi ft),$$
$$\frac{d^2y}{dt^2} = -A_y(2\pi f)^2\sin(2\pi ft) \tag{5}$$

then there are relationships between the dimensionless force coefficients in Eqs. (4*a*)–(4*c*). These are

$$C_{mv} = 2\pi^3\left(\frac{fD}{U}\right)^2\frac{A_y}{D}C_a \tag{6a}$$

$$C_{dv} = \frac{32\pi}{3}\left(\frac{A_y}{D}\frac{fD}{U}\right)^2 C_D \tag{6b}$$

and if the stationary cylinder shedding frequency equals the oscillation frequency $f_s = f$ then

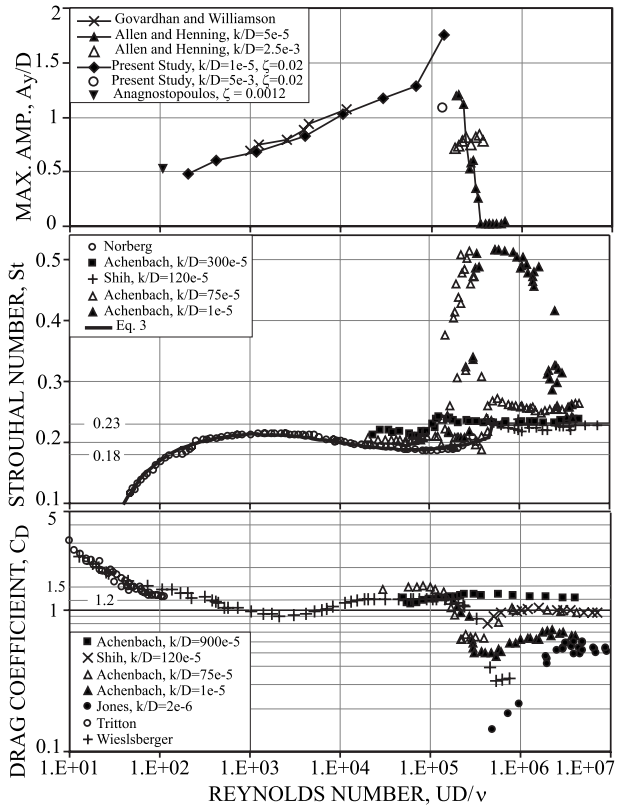

Fig. 2 Maximum transverse amplitude of lightly damped elastically supported cylinders, Strouhal number, and drag coefficient of stationary cylinders as functions of Reynolds number [6,12,18–22]. Equations (1)–(3). At top, $2^{1/2}$ was used to convert rms to peak in Ref. [18].

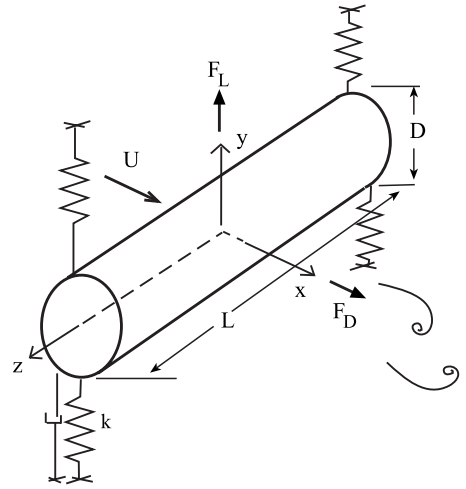

Fig. 3 Idealized spring supported damped cylinder

$$C_L\cos\varphi = C_{mv}, \quad C_L\sin\varphi = -C_{dv}, \quad C_L^2 = C_{mv}^2 + C_{dv}^2$$
$$C_{mv} = (1-(\mathrm{St}U/f_nD)^2)C_L/\sqrt{[(1-(\mathrm{St}U/f_nD)^2\ ]^2 + (2\zeta_n\mathrm{St}U/f_nD)^2} \tag{7}$$
$$C_{dv} = -2\zeta_n(\mathrm{St}U/f_nD)C_L/\sqrt{[(1-(\mathrm{St}U/f_nD)^2\ ]^2 + (2\zeta_n\mathrm{St}U/f_nD)^2}$$

The C_{dv} relationship in Eq. (6*b*) applies to the first Fourier series term for oscillating drag $|\cos\omega t|\cos\omega t \approx (8/3\pi)\cos\omega t$. The phase φ in Eq. (7) comes from Eq. (19*a*). Measured values of C_{mv} in the paper are normalized to zero for still water added mass $C_a = 1$.

Flow visualization experiments [2,25,26] and force and response measurements [6,29] show that the vortex wake and the dimensionless coefficients C_a, C_D, C_{mv}, and C_{dv} are functions of A_y/D and $\mathrm{St}U/fD$. Experiments [4,29–37] have measured the fluid force on cylinders undergoing forced motion in a flow. An alternate approach is taken here. C_a, C_D, C_{mv}, and C_{dv} are computed from a test program of natural vortex-induced vibration [19,38].

3 Added Mass and Fluid Damping From Free Decay Measurements

Consider the free decay of a damped elastically supported cylinder (Fig. 3) in a fluid modeled with Eq. (4*a*). The equation of motion of cylinder displacement $y(t)$ is

$$m_o\ddot{y} + 2m_o\zeta_o(2\pi f_o)\dot{y} + m_o(2\pi f_o)^2 y = F_y = -(1/2)\rho|\dot{y}|\dot{y}DC_D - \rho(\pi/4)D^2C_a\ddot{y} \tag{8}$$

where structural quantities are on the left, while fluid forces are on the right, and m_o is the dry mass of cylinder per unit length. Linearization of the nonlinear drag term, as performed earlier, allows an exact solution for the decaying oscillations with $\zeta < 1$ [39].

$$y(t) = A_y e^{-\zeta(2\pi f)t}\cos 2\pi f(1-\zeta^2)^{1/2}t \tag{9a}$$

$$\zeta = \zeta_o\frac{m_o}{m}\frac{f_o}{f} + \frac{2}{3\pi}\frac{\rho D^2}{m}\frac{A_y}{D}C_D, \quad f = f_o\sqrt{\frac{m_o}{m_o + \rho(\pi/4)D^2C_a}} \tag{9b}$$

An elastically suspended cylinder with a diameter of 6.35 cm [19] was off set and released in an otherwise still water. Measured amplitudes A_{yi} $(i=1,2,3\ldots N)$ of successive cycles during free decay were used to determine damping $\zeta = [1/(2\pi N)]\ln(A_i/A_{i+N})$. The corresponding frequencies f_i $(i=1,2,3\ldots N)$ are the inverse

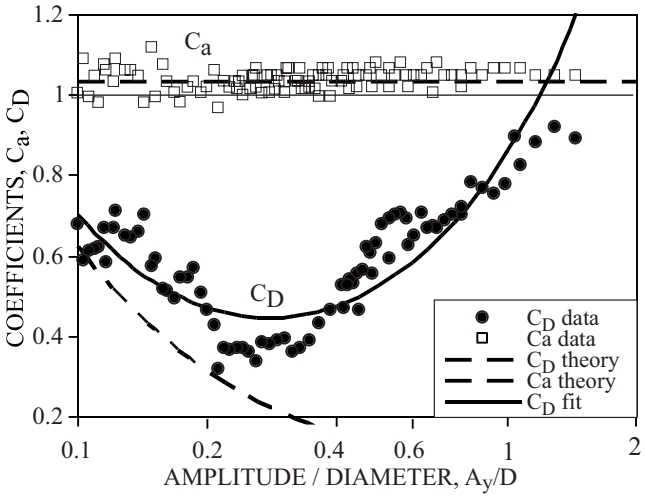

Fig. 4 Added mass and drag coefficients measured in still water in comparison with theory (Eq. (11))

of the time between successive peaks. These were used with Eq. (9*b*) to compute the added mass and drag coefficients of the oscillating cylinder as a function of its amplitude.

$$C_a = \frac{4}{\pi}\frac{m_o}{\rho D^2}\left[\left(\frac{f_o}{f}\right)^2 - 1\right], \quad C_D = \frac{3\pi}{2}\frac{m}{\rho D^2}\frac{D}{A_y}\left(\zeta - \zeta_o\frac{f_o}{f}\frac{m_o}{m}\right) \tag{10}$$

In air $f_o \approx 1.3$ Hz and $\zeta_o \approx 0.002$. There is also a stiffness correction for cylinder buoyancy.

Values of C_D and C_a measured in still water ($fD^2/\nu = 4550$, $\nu = 1.08\times10^{-6}$ m^2/s, $f \sim 1.2$ Hz, $D = 6.35$ cm) are plotted in Fig. 4 in comparison with theoretical viscous fluid solutions [40,41]

$$C_a = 1 + 4(\nu/\pi D^2 f)^{1/2} + (\nu/\pi D^2 f)^{3/2}, \tag{11a}$$

$$C_D = (3\pi^2/4)(D/A_y)(\nu/\pi D^2 f)^{1/2} \tag{11b}$$

The average measured added mass coefficient (1.038) is within 1% of the theoretical value (1.032). Measured drag coefficients exceed the theory, consistent with Refs. [42–44]. The drag coefficient has a minimum amplitude diameter near 0.3 cm [44,45]. C_D increases beyond diameter of 0.3, owing to separation and shed vortices [42–48]. The following expression correlates drag on oscillating cylinders in still water as the sum of viscous (Eq. (11*b*)) and amplitude-dependent components:

$$C_D = \frac{3\pi^{3/2}}{4}\frac{D}{A_y}\left(\frac{\nu}{fD^2}\right)^{1/2} + 0.8\frac{A_y}{D} \quad 0 < \frac{A_y}{D} < 1.5 \tag{12}$$

Next, the cylinder was off set transversely and released in water flowing at velocities from 15 cm/s to 92 cm/s. Measured cylinder damping and frequency in the initial decay are converted to fluid force coefficients C_{dv} and C_{mv} by the same process used for still water but starting with Eq. (15) instead of Eq. (8) to invoke the two parameter model. The following expressions correlate the measured C_{mv}, C_{dv}, and mean drag $C_D = 2F_D/\rho U^2 L$ for $1.5 > A_y/D > 0$ and $2.1 \geq \mathrm{St}U/fD \geq 0.4$ as functions of the cylinder amplitude and reduced velocity based on vibration frequency f.

$$C_{dv} = 0.4\pi(A_y/D)(fD/U) + (32\pi/3)(A_y/D)^2(fD/U)^2 C_{Do}$$

$$C_{mv} = F(\mathrm{St}U/fD)A_y/D \tag{13}$$

$$C_D = C_{Do} + 2(A_y/D)(1 - 0.45\mathrm{St}U/fD)$$

where C_{dv} is positive for the decaying oscillations. C_{mv} changes sign across resonance $\mathrm{St}U/fD \sim 1$. The function $F(\mathrm{St}U/fD)$ is approximated by line segments through points $(\mathrm{St}U/fD, F) = (0.3,0)$, $(0.6,1.25)$, $(1,1.25)$, $(1.05,-1.8)$ $(1.7,-1.8)$, $(3.5,0)$.

Hydrodynamic cylinder damping is obtained by substituting C_D (Eq. (12)) into Eq. (9*b*) for still water and C_{dv} (Eq. (13)) into Eq. (15) for water with freestream velocity U

$$\zeta_f = \begin{cases} \dfrac{\pi^{1/2}}{2}\dfrac{\rho D^2}{m}\left(\dfrac{\nu}{fD^2}\right)^{1/2} + \dfrac{1.6}{3\pi}\dfrac{\rho D^2}{m}\left(\dfrac{A_y}{D}\right)^2 & \text{for still fluid} \\ \dfrac{0.1}{4\pi}\dfrac{\rho D^2}{m}\dfrac{U}{fD} + \dfrac{2}{3\pi}\dfrac{\rho D^2}{m}\dfrac{A_y}{D}C_{Do} & \text{for moving fluid} \end{cases} \tag{14}$$

The first term in the moving fluid damping is similar in magnitude to that of Vandiver [49], but he does not include the second, amplitude-dependent, term. The still fluid damping expression is similar to that of Skop [44] but with a quadratic fit.

4 Fluid Force From Steady-State Response Measurements in Flowing Water

Measured cylinder amplitude and frequency during steady-state vortex-induced cylinder vibration are used to determine the vortex-induced fluid forces. The equation for steady self-excited vortex induced vibrations of an elastically supported cylinder (Fig. 3) in cross flow with the two parameter lift force model (Eq. (4*c*))

$$m\ddot{y} + 2m\zeta_n\omega_n\dot{y} + ky = F_y = \frac{1}{2}\rho U^2 D C_{mv}\sin(2\pi ft) - \frac{1}{2}\rho U^2 D C_{dv}\cos(2\pi ft) \tag{15}$$

is solved with Eq. (5) by separating in-phase and out-of-phase components to give C_{mv} and C_{dv} as functions of oscillation frequency f and cylinder amplitude A_y

$$C_{mv} = 8\pi^2\mathrm{St}^2\frac{m}{\rho D^2}\frac{A_y}{D}\left(1 - \frac{f^2}{f_n^2}\right)\left(\frac{\mathrm{St}U}{f_n D}\right)^{-2} \tag{16a}$$

$$C_{dv} = -4\pi\mathrm{St}^2\frac{2m(2\pi\zeta_n)}{\rho D^2}\frac{A_y}{D}\frac{f}{f_n}\left(\frac{\mathrm{St}U}{f_n D}\right)^{-2} \tag{16b}$$

where ζ_n is the structural damping factor measured in still air with the cylinder weighted to simulate the still water added mass.

Tests. Steady-state cylinder amplitude A_y and frequency f were measured during a series of tests with water velocities between 15 cm/s and 92 cm/s in steps of 1 cm/s, corresponding to $2 < U/f_n D < 12$ with a 6.35 cm (2.5 inch) diameter cylinder [19]. Reynolds number range from 10,000 to 80,000. At each velocity, the structural (magnetic) damping factor varied between 0.002 and 0.4 to achieve the target amplitudes A_y/D between 0.05 and 1.45 in steps of 0.1. Measured amplitude, frequency, and drag were converted to C_{mv}, C_{dv}, and C_D with Eqs. (2), (16*a*), and (16*b*).

Measured Coefficients. Triplets of $C_{mv}[A_y/D, \mathrm{St}U/fD]$, $C_{dv}[A_y/D, \mathrm{St}U/fD]$, and $C_D[A_y/D, \mathrm{St}U/fD]$ from approximately 1000 tests were reduced to a uniform grid by sorting them into $15\times18 = 270$ cells with A_y/D ranging from 0 to 1.5 in steps of 0.1 and $\mathrm{St}U/(fD)$ from 0.4 to 2.4 in steps of 0.1. Decay tests (described above as $C_{dv} > 0$) were used to fill cells for nonexcited cases.

A typical table cell has about four measured points. Every cell has at least one measured data point with the exception of the two cells centered at $A_y/D = 0.05$ and $1.4 < \mathrm{St}U/fD < 1.6$, where no response was observed; their values are interpolated. Tests on cell boundaries were removed and the cell average was taken. The results are shown in Tables 1–3 for transverse-only motion.

Trends can be seen in the tables. C_{mv} is positive for $f/f_n > 1$ and negative for $f/f_n < 1$. C_{dv} is negative for all cases with steady-

Table 1 C_{mv} for transverse motion

StU/fD Ay/D	0.5 to 0.6	0.6 to 0.7	0.7 to 0.8	0.8 to 0.9	0.9 to 1.0	1.0 to 1.1	1.1 to 1.2	1.2 to 1.3	1.3 to 1.4	1.4 to 1.5	1.5 to 1.6	1.6 to 1.7	1.7 to 1.8	1.8 to 1.9	1.9 to 2.0	2.0 to 2.1	2.1 to 2.2	2.2 to 2.3
0 to 0.1	0.032	0.082	0.106	0.086	0.100	-0.126	**-0.087**	-0.231	**-0.090**	**-0.090**	**-0.090**	**-0.090**	**-0.088**	**-0.083**	**-0.158**	**-0.134**	**-0.090**	**-0.094**
0.1 to 0.2	0.063	0.164	0.201	0.158	0.184	0.852	0.125	-0.337	**-0.463**	**-0.367**	**-0.292**	**-0.238**	**-0.376**	**-0.291**	**-0.255**	**-0.204**	**-0.194**	**-0.193**
0.2 to 0.3	0.119	0.278	0.350	0.273	0.312	0.852	1.237	0.162	**-0.433**	**-0.547**	**-0.471**	**-0.410**	**-0.486**	**-0.414**	**-0.398**	**-0.387**	**-0.320**	**-0.292**
0.3 to 0.4	0.145	0.408	0.501	0.394	0.465	**-0.101**	1.121	0.564	**-0.336**	**-0.626**	**-0.660**	**-0.581**	**-0.669**	**-0.587**	**-0.547**	**-0.527**	**-0.412**	**-0.438**
0.4 to 0.5	0.208	0.522	0.644	0.448	0.575	0.036	1.147	0.533	**-0.371**	**-0.675**	**-0.733**	**-0.672**	**-0.844**	**-0.757**	**-0.750**	**-0.658**	**-0.547**	**-0.616**
0.5 to 0.6	0.266	0.635	0.800	0.606	0.686	**-0.181**	1.279	0.535	**-0.421**	**-0.736**	**-0.870**	**-1.044**	**-1.069**	**-0.941**	**-0.916**	**-0.798**	**-0.708**	**-0.735**
0.6 to 0.7	0.323	0.781	0.953	0.573	0.815	**-0.366**	1.552	0.544	**-0.547**	**-0.801**	**-0.878**	**-1.250**	**-1.284**	**-1.111**	**-1.085**	**-0.996**	**-0.815**	**-0.838**
0.7 to 0.8	0.423	0.855	1.085	0.789	0.945	**-0.190**	**-1.475**	0.504	**-0.540**	**-0.710**	**-1.140**	**-1.459**	**-1.457**	**-1.270**	**-1.226**	**-1.138**	**-0.941**	**-0.970**
0.8 to 0.9	0.506	0.964	1.252	0.929	1.116	**-0.194**	**-1.597**	0.466	**-0.569**	**-1.362**	**-1.291**	**-1.614**	**-1.656**	**-1.452**	**-1.390**	**-1.289**	**-1.093**	**-1.096**
0.9 to 1.0	0.609	1.100	1.359	0.998	1.220	**-0.316**	1.500	0.483	**-0.181**	**-1.580**	**-1.440**	**-1.793**	**-1.845**	**-1.623**	**-1.553**	**-1.441**	**-1.217**	**-1.225**
1.0 to 1.1	0.514	1.233	1.574	1.182	1.338	**-0.455**	0.909	0.357	**-0.345**	**-1.748**	**-1.583**	**-1.998**	**-2.040**	**-1.807**	**-1.706**	**-1.588**	**-1.347**	**-1.374**
1.1 to 1.2	0.755	1.331	1.670	1.267	1.407	**-0.284**	0.446	-0.010	**-0.401**	**-1.898**	**-1.747**	**-2.158**	**-2.280**	**-1.945**	**-1.880**	**-1.726**	**-1.462**	**-1.485**
1.2 to 1.3	0.818	1.447	1.815	1.253	1.604	**-0.126**	**-2.374**	**-2.351**	**-1.634**	**-2.077**	**-1.879**	**-2.379**	**-2.468**	**-2.163**	**-2.044**	**-1.896**	**-1.611**	**-1.594**
1.3 to 1.4	0.888	1.563	1.961	1.571	1.733	**-0.333**	**-2.564**	**-2.539**	**-1.759**	**-2.239**	**-2.061**	**-2.551**	**-2.603**	**-2.297**	**-2.207**	**-2.048**	**-1.729**	**-1.741**
1.4 to 1.5	0.370	1.696	2.117	1.528	1.855	**-0.668**	**-2.934**	**-2.774**	**-1.897**	**-2.382**	**-2.233**	**-2.758**	**-2.817**	**-2.477**	**-2.371**	**-2.200**	**-1.866**	**-1.870**

Table 2 C_{dv} for transverse motion

StU/fD Ay/D	0.5 to 0.6	0.6 to 0.7	0.7 to 0.8	0.8 to 0.9	0.9 to 1.0	1.0 to 1.1	1.1 to 1.2	1.2 to 1.3	1.3 to 1.4	1.4 to 1.5	1.5 to 1.6	1.6 to 1.7	1.7 to 1.8	1.8 to 1.9	1.9 to 2.0	2.0 to 2.1	2.1 to 2.2	2.2 to 2.3
0 to 0.1	0.062	0.051	0.034	0.022	0.054	**-0.661**	**-0.423**	**-0.176**	0.010	0.009	0.009	0.008	0.008	0.007	0.005	0.005	0.011	0.018
0.1 to 0.2	0.163	0.158	0.086	0.057	0.108	**-0.021**	**-0.563**	**-0.365**	**-0.238**	**-0.075**	**-0.033**	**-0.015**	0.014	0.011	0.009	0.016	0.053	0.034
0.2 to 0.3	0.388	0.347	0.232	0.137	0.272	**-0.021**	**-0.014**	**-0.461**	**-0.300**	**-0.112**	**-0.042**	**-0.006**	0.019	0.024	0.018	0.062	0.098	0.064
0.3 to 0.4	0.578	0.537	0.390	0.236	0.383	0.200	**-0.017**	**-0.666**	**-0.342**	**-0.222**	**-0.047**	**-0.026**	0.032	0.035	0.089	0.088	0.122	0.139
0.4 to 0.5	0.894	0.687	0.502	0.513	0.398	0.199	**-0.230**	**-0.636**	**-0.336**	**-0.209**	**-0.040**	**-0.010**	0.104	0.153	0.226	0.162	0.209	0.269
0.5 to 0.6	1.282	0.984	0.754	0.580	0.494	0.240	**-0.197**	**-0.641**	**-0.354**	**-0.177**	**-0.034**	0.166	0.472	0.405	0.402	0.419	0.351	0.329
0.6 to 0.7	2.207	1.522	1.001	0.823	0.614	0.624	**-0.044**	**-0.595**	**-0.316**	**-0.094**	**-0.025**	0.151	0.399	0.337	0.390	0.420	0.350	0.284
0.7 to 0.8	3.148	1.710	1.224	0.901	0.704	0.958	0.287	**-0.597**	**-0.212**	**-0.027**	0.446	0.574	0.501	0.790	0.677	0.615	0.467	0.426
0.8 to 0.9	3.610	2.538	1.951	1.397	0.772	0.992	0.873	**-0.546**	**-0.134**	0.531	0.475	0.649	0.644	0.742	0.852	0.775	0.615	0.438
0.9 to 1.0	5.130	3.618	2.314	1.608	1.514	1.564	**-0.090**	**-0.441**	**-0.399**	0.483	0.676	0.647	0.833	0.981	0.953	0.866	0.777	0.539
1.0 to 1.1	6.387	4.465	3.588	2.317	1.971	1.767	**-0.066**	**-0.303**	**-0.220**	0.801	0.622	0.737	0.955	0.998	1.478	1.072	0.818	0.744
1.1 to 1.2	6.210	4.380	3.257	2.840	2.095	1.874	**-0.052**	**-0.053**	**-0.064**	0.544	0.918	0.864	1.168	1.196	1.470	1.270	1.160	0.830
1.2 to 1.3	6.750	4.761	3.542	3.197	2.508	2.150	1.910	1.685	1.491	1.060	0.810	0.827	1.299	1.187	1.597	1.595	1.193	0.876
1.3 to 1.4	8.747	6.170	4.099	3.728	2.786	2.309	2.062	1.820	1.571	1.299	1.231	1.024	1.405	1.471	1.928	1.845	1.379	1.008
1.4 to 1.5	9.700	6.577	4.161	4.687	3.583	2.765	2.243	1.908	2.009	1.551	1.381	1.123	1.759	1.729	2.181	1.982	1.552	1.082

Table 3 C_D for transverse motion

StU/fD Ay/D	0.5 to 0.6	0.6 to 0.7	0.7 to 0.8	0.8 to 0.9	0.9 to 1.0	1.0 to 1.1	1.1 to 1.2	1.2 to 1.3	1.3 to 1.4	1.4 to 1.5	1.5 to 1.6	1.6 to 1.7	1.7 to 1.8	1.8 to 1.9	1.9 to 2.0	2.0 to 2.1	2.1 to 2.2	2.2 to 2.3
0 to 0.1	1.16	0.96	0.93	0.96	1.13	1.07	1.11	1.09	1.11	1.11	1.10	1.11	1.10	1.09	1.13	1.06	1.08	1.01
0.1 to 0.2	1.23	0.98	0.94	1.03	0.93	1.13	1.16	1.09	1.13	1.15	1.15	1.15	1.00	1.00	1.12	1.10	1.11	1.03
0.2 to 0.3	1.31	1.02	0.98	1.09	1.07	1.36	1.36	1.25	1.18	1.19	1.19	1.19	1.06	1.03	1.14	1.16	1.16	1.07
0.3 to 0.4	1.42	1.09	1.04	1.18	1.14	1.56	1.51	1.44	1.27	1.24	1.23	1.20	1.12	1.06	1.19	1.21	1.18	1.13
0.4 to 0.5	1.52	1.17	1.11	1.34	1.32	1.60	1.69	1.63	1.41	1.33	1.24	1.20	1.19	1.12	1.24	1.23	1.24	1.23
0.5 to 0.6	1.68	1.26	1.22	1.44	1.47	1.76	1.73	1.78	1.57	1.51	1.32	1.26	1.29	1.19	1.32	1.29	1.31	1.19
0.6 to 0.7	1.87	1.07	1.34	1.64	1.57	1.93	1.81	1.93	1.74	1.64	1.44	1.39	1.39	1.25	1.35	1.36	1.35	1.25
0.7 to 0.8	2.00	1.49	1.46	1.77	1.71	1.99	2.41	2.09	1.92	1.80	1.64	1.50	1.47	1.30	1.41	1.40	1.41	1.30
0.8 to 0.9	2.01	1.62	1.63	1.97	1.89	2.12	2.54	2.32	2.08	1.93	1.77	1.59	1.56	1.36	1.46	1.45	1.47	1.34
0.9 to 1.0	2.24	1.81	1.76	2.16	2.00	2.27	2.65	2.84	2.47	2.08	1.90	1.69	1.64	1.42	1.51	1.51	1.51	1.38
1.0 to 1.1	2.53	2.02	2.05	2.29	2.13	2.39	3.03	3.06	2.65	2.23	2.03	1.81	1.73	1.49	1.56	1.55	1.56	1.43
1.1 to 1.2	2.69	2.18	2.19	2.73	2.33	2.48	3.33	3.32	2.91	2.37	2.18	1.92	1.79	1.54	1.62	1.60	1.62	1.47
1.2 to 1.3	2.94	2.39	2.42	2.67	2.41	2.60	3.17	3.06	2.90	2.52	2.29	2.02	1.89	1.62	1.67	1.66	1.67	1.51
1.3 to 1.4	3.21	2.62	2.67	2.93	2.55	2.73	3.32	3.22	3.02	2.67	2.46	2.12	1.98	1.66	1.73	1.71	1.70	1.56
1.4 to 1.5	3.47	2.90	2.96	2.93	2.68	2.95	3.51	3.41	3.15	2.80	2.61	2.24	2.08	1.72	1.78	1.76	1.77	1.60

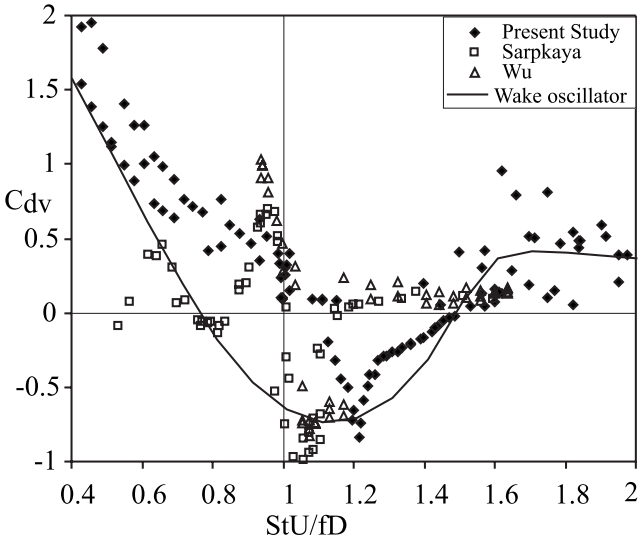

Fig. 5 Measured C_{dv} with StU/fD compared with forced vibration test data [29,50] for $0.5<A_y/D<.6$ and wake oscillator model (Eq. (24))

state cylinder response; it becomes positive at large amplitude, creating damping and limiting the maximum amplitude of vortex-induced vibrations. Negative values of C_{dv} occur between $1 \leq \mathrm{St}U/fD < 1.6$ so large amplitude oscillations have frequencies between the 70% and 100% of the stationary shedding frequency (Fig. 3 (top) [19]). This implies that large extensive entrainment is only possible if the oscillation frequency follows the shedding frequency upward as velocity increases [19]. Measured C_{dv} in Fig. 5 compare well with forced oscillations experiments [29,50] and measured steady drag at maximum resonant response compares well with the correlation of Sparkaya [29] in Fig. 6.

Intermediate values of C_{mv} and C_{dv} are biharmonically interpolated from the tabulated values. For example, C_{mv} at A_y/D and StU/fD is interpolated from the four surrounding C_{mv} values V_1, V_2, V_3, and V_4 counting clockwise from the upper left in Table 1, $a=(V_1+V_2+V_3+V_4)/4$, $b=(-V_1-V_2+V_3+V_4)/2$, $c=(-V_1+V_2+V_3-V_4)/2$, and $d=(V_1-V_2+V_3-V_4)/2$, that is

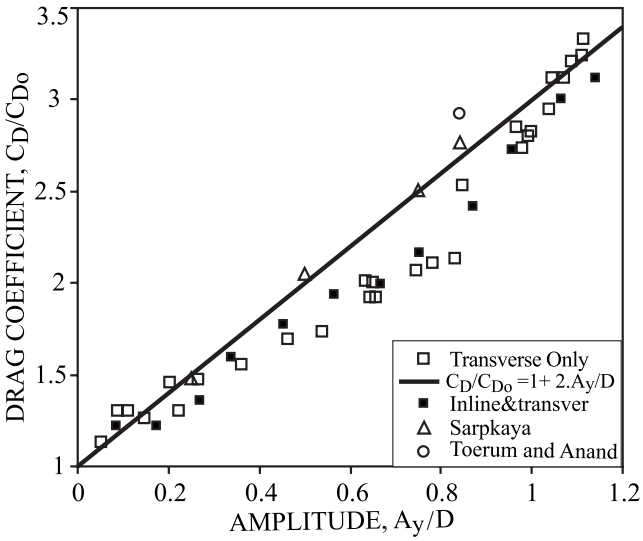

Fig. 6 Drag coefficient at maximum response amplitude: present data, Ref. [19], and Refs. [29,51].

$$C_{mv}(A_y/D, \mathrm{St}U/fD) = a + br + cs + drs, \quad -0.5 \leq r,s < 0.5 \tag{17}$$

where r and s are values of A_y/D and StU/fD relative to their values at the center of the surrounding four table cells, divided by the table grid spacing of 0.1. Below the diameter of 0.05, a table row corresponding to $A_y/D=-0.05$ is created by repeating the row at $A_y/D=+0.05$ or alternately with the lift coefficient model (Eq. (7)) or wake oscillator model (Eqs. (22*a*), (22*b*), and (24)) can be applied. Figures 8 and 9 were created using the first approach.

5 Prediction of Vortex-Induced Vibration Using the Measured Forces

The fluid forces measured in Sec. 4 are applied to the prediction of transverse vortex-induced vibration of circular cylinders using the (1) lift coefficient, (2) two parameter, and (3) wake oscillator models.

5.1 Constant C_L Model. The equation of transverse motion of a spring supported cylinder responding (Fig. 2) to the constant lift coefficient force (Eq. (4*b*)) at the stationary cylinder shedding frequency $f=f_s|_{\mathrm{Eq.\ 1}}$ has an exact steady-state harmonic solution (Eq. (5)) [39] as follows:

$$m\ddot{y} + 2m\zeta_n\omega_n\dot{y} + ky = F_y = (1/2)\rho U^2 D C_L \sin(2\pi f_s t + \varphi) \tag{18}$$

$$f_s = \mathrm{St}U/D, \quad f_n = (1/2\pi)(k/m)^{1/2}, \quad f_s/f_n = \mathrm{St}U/f_n D$$

$$\frac{A_y}{D} = \frac{C_L}{8\pi^2}\frac{\rho D^2}{m}\left(\frac{U}{f_n D}\right)^2\left[\left(1-\frac{f_s^2}{f_n^2}\right)^2 + \left(\frac{2\zeta_n f_s}{f_n}\right)^2\right]^{-1/2} \tag{19a}$$

$$= \frac{C_L}{4\pi \mathrm{St}^2 \delta_r} \text{ at } f_n = f_s \text{ where } \varphi = \frac{\pi}{2} \tag{19b}$$

$$\tan\varphi = \frac{2\zeta_n f_s/f_n}{1-f_s^2/f_n^2}, \quad \delta_r = \frac{2m(2\pi\zeta_n)}{\rho D^2} \tag{19c}$$

The cylinder response amplitude A_y is proportional to the lift coefficient C_L divided by the mass ratio $m/\rho D^2$. $C_L=1$ with St $=0.2$ bounds transverse response data in Fig. 9 but $C_L=0.7$ is a better fit to low amplitude data in Figs. 7 and 8. At small amplitudes the finite spanwise correlation length l_c of vortex shedding, often between diameters of 3 and 7 for a stationary cylinder, reduces the root mean square lift by the factor $(l_c/L)^{1/2}$ [7,9,10,25,38,51–53].

The constant C_L model accurately predicts experimental data below 0.05 diameter amplitude, but it lacks the rightward shift of maximum response, entrainment, and self-limiting response at larger amplitudes. These shortcomings are addressed by the amplitude and frequency dependent coefficients C_{mv} $(A_y/D, \mathrm{St}U/fD)$ and C_{dv} $(A_y/D, \mathrm{St}U/fD)$ of Tables 1 and 2, as used in the two parameter model (Sec. 5.2).

In 1956, Scruton introduced dimensionless reduced mass damping $\delta_r=2m(2\pi\zeta)/\rho D^2$ (Eq. (19*c*)) to correlate the maximum amplitude of cylinders in the wind [54,55] and this predates the 1973 application of the monogram $S_G=(2\pi\mathrm{St})^2\delta_r$ by Skop and Balasubramanian [56] and Griffin et al. [57] to offshore piping. References [6,10,53,57,58] have correlations for $A_{y\,\max}$ with δ_r and S_G. Figure 7 uses a log scale to show both high and low amplitude behaviors of data and two correlations—Eq. (29) and $A_y/D=[1-1.124\delta_r/\pi^2+0.296(\delta_r/\pi^2)^2)]\log_{10}(0.41\,\mathrm{Re}^{0.36})$ [6]—for maximum amplitude as function of δ_r. The latter expression fits in the upper range and addresses the Reynolds number effects but it crosses zero twice for $\delta_r>10$.

5.2 Two Parameter Force Model at Steady-State. Steady-state solutions to the two parameter model are sought by inverting

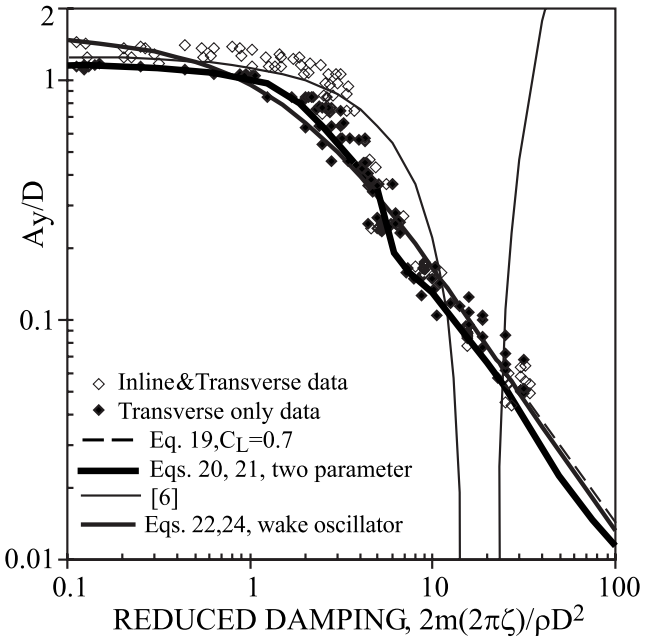

Fig. 7 Scruton plot of resonant transverse amplitude versus reduced damping. Dark solid line is two parameter (Eqs. (20) and (21)) solution with Tables 1 and 2 and St=0.21.

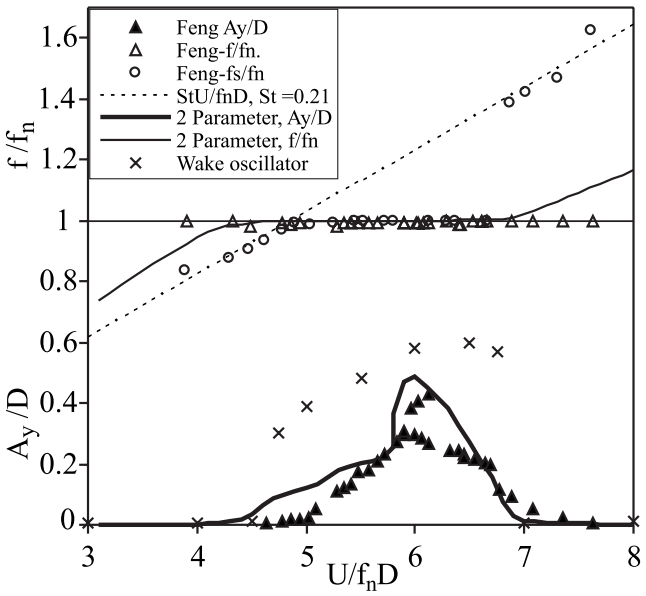

Fig. 9 Comparison of predicted response amplitude (—) (Eqs. (20) and (21)) using data from Tables 1 and 2 as a function of velocity with data from spring supported rigid cylinder tests in air [59]

the measurement equations (Eq. (16)), and solving the two coupled nonlinear equations for cylinder amplitude A_y and frequency f

$$\mathrm{St}^2\frac{A_y}{D}\left[1-\frac{f^2}{f_n^2}\right]=\frac{1}{4\pi^2}\frac{\rho D^2}{2m}\left(\frac{\mathrm{St}U}{f_nD}\right)^2 C_{mv}\left[\frac{A_y}{D},\frac{\mathrm{St}U}{fD}\right] \tag{20}$$

$$4\pi\mathrm{St}^2\frac{2m(2\pi\zeta_n)}{\rho D^2}\frac{A_y}{D}\frac{f}{f_n}=-\left(\frac{\mathrm{St}U}{f_nD}\right)^2 C_{dv}\left[\frac{A_y}{D},\frac{\mathrm{St}U}{fD}\right] \tag{21}$$

Substituting the biharmonic interpolation (Eq. (17)) for C_{mv} into Eq. (20) produces a cubic equation in terms of f/f_n with exact solutions for f given A_y/D that are substituted into Eq. (21),

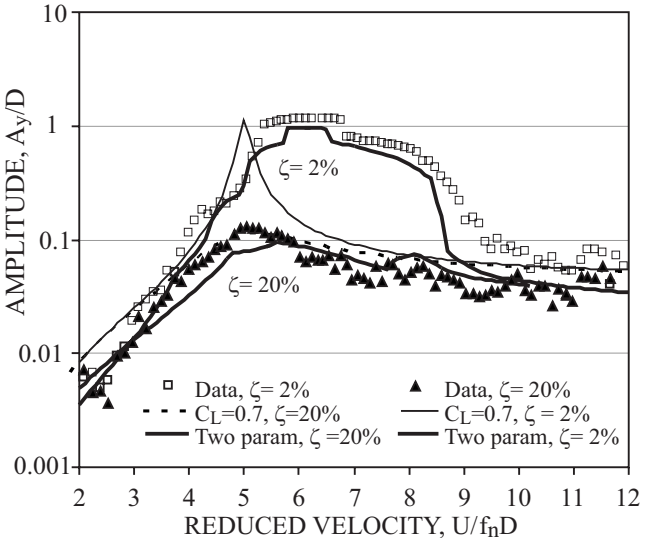

Fig. 8 Vortex-induced cylinder response predicted by lift coefficient model (Eq. (19)) with C_L=0.7, and two parameter coupled model (Eqs. (20) and (21)) using Tables 1 and 2 data in comparison with experimental data; $\rho D^2/(2m)$=0.1 and St =0.21

which is then numerically searched for amplitudes A_y/D in the interpolation range of each cell. Multiple solutions, some unstable, can exist. Once A_y and f are known, the mean drag coefficient is read from Table 3. Figure 8 shows the two parameter model solution reproduces entrainment and self-limiting effects for lightly damped cylinders responding at large amplitude. At zero structural damping Eq. (21) becomes $C_{dv}[A_y/D,\mathrm{St}U/fD]=0$, which is outlined in Table 2.

Figure 8 shows that the two parameter model (Eqs. (20) and (21) with Tables 1 and 2) predictions agree with the measured data. Figure 9 compares the two parameter numerical solution with the data of Feng [59] for transverse motion of a spring supported two dimensional cylinder (Fig. 3) for $\rho D^2/2m$=0.00257, ζ_n=0.00145, δ_r=3.54, and St=0.21. Note that his experiment in air is at $\frac{1}{38}$ of the mass ratio of the present experiments.

5.3 Wake Oscillator Model. Wake oscillator model for vortex-induced vibration is a self-excited, single degree of freedom van der Pol oscillator model of near wake fluid coupled to transverse cylinder vibrations [10,56,60,62–64]

$$a_0\rho D^2\ddot{z}+a_0\rho D^2\omega_{s1}^2 z=(a_1-a_{41})\rho UD\dot{z}-a_2\rho D\dot{z}^3/U+a_{42}\rho UD\dot{y} \tag{22a}$$

$$\omega_{s1}^2=a_0\rho D^2\omega_s^2 a_6/(1+a_5(z^2+\dot{z}^2/\omega_s^2)^{1/2}/D) \tag{22b}$$

$$m\ddot{y}+2\zeta m\omega_y\dot{y}+ky=F_y=a_{43}\rho UD\dot{z}-a_{44}\rho UD\dot{y} \tag{22c}$$

where z represents the fluid degree of freedom. This formulation is same as in Refs. [10,61] but with coefficients a_0=0.48, a_1=0.44, a_2=0.2, a_3=0, and a_4 expanded to four coefficients, namely, a_{41}=0.35, a_{42}=1, a_{43}=0.4, and a_{44}=0.5, to increase the entrainment and fit data in Figs. 5 and 7. A softening spring a_5=0.3 and $a_6=1+a_5A_{z0}/D$ shifts the resonance to the right at higher amplitude.

Harmonic solutions ($z=A_z\sin\omega t$) are sought by expanding the cubic $\cos^3\omega t=(3/4)\cos\omega t-(1/4)\cos 3\omega t$ and retaining only the first term. For a stationary cylinder (y=0), this gives

$$z = A_{zo}\cos\omega_s t,\quad A_{zo} = ((4(a_1 - a_{41})/3a_2)^{1/2}/2\pi S$$
$$F_y = a_{43}\rho UDz = (1/2)\rho U^2(4\pi \mathrm{St} a_{43}A_{zo}),\ \text{hence}\ C_L = 4\pi \mathrm{St} a_{43}A_{zo} \tag{23}$$

With St=0.2 and the above parameters $A_{zo}/D=0.616$ and $C_L=0.62$, the wake oscillator and lift coefficient model are nearly identical for predictions of the lift force and response (Fig. 7) at small amplitudes. The wake oscillator has entrainment and self-limiting response at higher amplitude.

For forced cylinder motion $y(t)=A_y \sin \omega t$ (Eq. (5)) at circular frequency ω (Eq. (23)) becomes a classical forced van der Pol oscillator. The solution (see Appendix) is

$$z = b_1\cos\omega t + b_2 \sin\omega t$$
$$C_{mv} = -4\pi \mathrm{St} a_{43}(\omega/\omega_s)(b_1/D), \tag{24}$$
$$C_{dv} = 4\pi \mathrm{St}(\omega/\omega_s)(a_{43}b_2/D - a_{44}A_y/D)$$

The result for C_{dv} is shown in comparison with the data in Fig. 5.

5.4 Application to Continuous Structures. Galerkin modal analysis [61,65] is applied to the partial differential equation of motion of a slender elastic structure responding to the transverse forces of Eq. (4*c*) to reduce it to a single degree of freedom that is solved using the previous procedure.

$$L[Y(z,t)] + m(z)\frac{\partial^2 Y(z,t)}{\partial t^2} = \frac{1}{2}\rho U^2 D C_{mv}\sin(2\pi ft) - \frac{1}{2}\rho U^2 D C_{dv}\cos(2\pi ft) \tag{25}$$

The displacement $Y(z,t)$ is a function of time t and longitudinal span z, and $L[Y(z,t)]$ is the differential stiffness operator. Harmonic response in a single mode, which is the ith mode, is expressed as a one term series

$$Y(z,t) = A_{yi}y_i(z)\sin(2\pi ft) \tag{26}$$

that is substituted into Eq. (25), which is then multiplied through by $y_i(x)$, and integrated over the span. For a uniform diameter and flow, modal force coefficients C_{mvi} and C_{dvi} can be defined.

$$C_{mvi} = \frac{\int_0^L C_{mv}[\mathrm{St}U/fD, A_y/D]|y_i(z)|dz}{\int_0^L y_i^2(z)dz},$$
$$C_{dvi} = \frac{\int_0^L C_{dv}[\mathrm{St}U/fD, A_y/D]|y_i(z)|dz}{\int_0^L y_i^2(z)dz} \tag{27}$$

Modal analysis reduces Eq. (25) to Eqs. (20) and (21) with redefinitions of Eq. (27) of the fluid force coefficients, so the previous solution method applies. Still fluid drag-damping can be incorporated by replacing Eq. (4*c*) with Eq. (4*a*) for portions of the cylinder in still water.

When applied to the wake oscillator model (Eq. (22)), with $a_5=0$ and $a_6=0$, this modal procedure results in the following expression for maximum resonant response:

$$\frac{A_y}{D} = \frac{a_{43}(4/3)^{1/2}\gamma}{2\pi \mathrm{St}^2(\delta_r + a_{44}/\mathrm{St})}\sqrt{\frac{a_1 - a_{41}}{a_2} + \frac{a_{42}a_{43}}{a_2 \mathrm{St}(\delta_r + a_{44}/\mathrm{St})}} = \frac{0.0735\gamma}{\mathrm{St}^2(\delta_r + 0.5/\mathrm{St})}\sqrt{0.45 + \frac{2}{\mathrm{St}(\delta_r + 0.5/\mathrm{St})}} \tag{28}$$

The dimensionless modal parameter $\gamma=1$ for a rigid two dimensional motion (Fig. 3, $\gamma=1.155$ for a sinusoidal mode shape, and $\gamma=1.291$ for a pivoted cantilever, where A_y now refers to the maximum amplitude along the mode shape [10,62].

5.5 Time History Solutions. The equation of motion can be numerically integrated step-by-step in time. The two parameter mode (Eq. (15)) is put in suitable form [66] using Eq. (5).

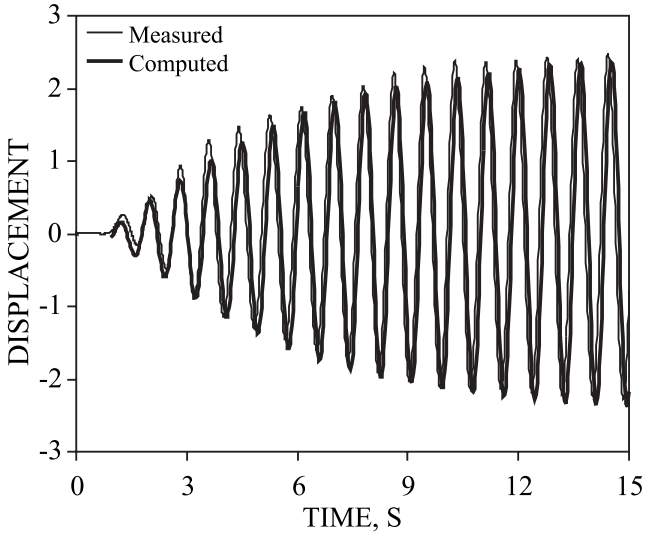

Fig. 10 Transient prediction with two parameter model (Eqs. (30), (31), and (17)) (Tables 1 and 2) and measured transient response; $\rho D^2/m=0.2$, $\varsigma=0.02$. St=0.205, $U/f_nD=6.21$

$$\left(m + \frac{1}{2}\rho U^2 D C_{mv}/\omega^2 A_y\right)\ddot{y} + \left(2m\zeta_n\omega_n + \frac{1}{2}\rho U^2 D C_{dv}/\omega A_y\right)\dot{y} + ky = 0 \tag{29}$$

where C_{mv} and C_{dv} at the current step are evaluated with Tables 1 and 2 and Eq. (17) using the amplitude and frequency estimated from the previous time, that is

$$f_n^2/f^2 = 1 + (1/(8\pi^2))(\rho D^2/m)(U/fD)^2(D/A_y)C_{mv}[A_y/D, \mathrm{St}U/fD] \tag{30a}$$
$$A_y^2 = y(t)^2 + y(t)^2/(2\pi f)^2 \tag{30b}$$

Figure 10 is a computed startup of a cylinder released in a steady flow in comparison with the data. Time history analysis can be extended to continuous structure, multiple mode responses, or direct integration, using the autocorrelation of previous time history

$$R_{yy}(\tau) = \frac{1}{t_1 - t_2}\int_{t1}^{t2} y(t)y(t+\tau)dt,\quad 0 < \tau < (t_1 - t_2) \tag{31}$$

to determine frequency f and amplitude of the dominant amplitude A_y in the entrainment range of frequencies, based on negative $C_{dv}<0$ (Table 1) and experiments [19]

$$f_s/1.6 < f < f_s \tag{32}$$

The corresponding phase is found from the Fourier series expansion of the previous time history at this frequency. An initial offset can be applied to start the solution, or alternately, the wake oscillator or lift coefficient model, could be applied.

6 Conclusions

Oscillating vortex-induced lift coefficients in-phase (C_{mv}) and out-of-phase (C_{dv}) with cylinder motion and mean drag (C_D) have been determined for cylinder amplitudes from 0.05 to 1.5 diameters and reduced velocities between 2 cm/s and 12 cm/s, by post-processing a large number of experiments for response of elastically supported cylinders in water flow. These force coefficients have been reduced to a uniform tabular grid as functions of non-dimensional frequency and amplitude of cylinder motion and employed in predictive models for vortex-induced vibration.

1. The oscillating lift forced model (Eqs. (18) and (19)) with $C_L=0.7$ is a good fit to data for small amplitude vortex-induced vibration, $Ay/D<0.5$.
2. Moderate and large amplitude vortex-induced vibrations are well represented by the two parameter model (Eqs. (4*c*), (15), (20), and (21)). It has good agreement for steady-state and transient cylinder response in both water and air, including frequency entrainment, large amplitude response, and self-limiting amplitudes greater than one diameter. However, for transient analysis it requires tracking of the dominant amplitude and frequency of the response.
3. The wake oscillator model (Eq. (22*a*)–(22*c*)) with tuned coefficients reproduces entrainment, self-limiting amplitude, and frequency shift. It envelopes the data from small to large amplitudes, but it does not reproduce the finer details of cylinder response.
4. The negative values of C_{dv} fall in the range $1 \leq \mathrm{St}U/fD < 1.6$. This implies that extensive entrainment is only possible if the oscillation frequency f follows the shedding frequency upward from the cylinder natural frequency, $f > 0.9f_n$, as velocity increases.

Nomenclature

- A_y = amplitude of vibration transverse to tube axis and flow
- C_a = added mass coefficient, dimensionless (Eqs. (4*a*) and (11))
- C_L = lift coefficient, dimensionless (Eq. (4*b*))
- C_{Do} = drag coefficient for stationary cylinder in steady flow, dimensionless (Eq. (2))
- C_{dv} = oscillating negative damping coefficient, dimensionless (Eq. (4*c*))
- C_{mv} = oscillating inertia coefficient, normalized to zero for still water added mass, dimensionless (Eq. (4*c*))
- D = cylinder outside diameter
- F_D = mean drag on the cylinder
- F_y = transverse force, transverse to flow, per unit length of cylinder
- L = wetted span of cylinder
- $\mathrm{Re}=UD/\nu$ = Reynolds number, dimensionless
- St = Strouhal number for stationary cylinder, dimensionless (Eq. (1))
- U = freestream flow velocity
- f = cylinder oscillation frequency, generally differs from f_o, f_s, or f_n (Hz)
- f_o = natural frequency in still air (Hz)
- f_n = natural frequency in still water, $(\mathrm{k/m})^{1/2}/2\pi$ (Hz)
- f_s = vortex shedding frequency from stationary cylinder (Hz) (Eq. (1))
- k = surface roughness of cylinder (Fig. 2) or spring constant per unit length
- m_o = dry mass of cylinder and moving suspension in air per unit length
- m = mass per unit length of cylinder with still water added mass, $m_o+\rho(\pi D^2/4)C_a$
- $m/\rho D^2$ = mass ratio, dimensionless
- t = time
- y = direction perpendicular to freestream flow, transverse
- $y(t)$ = displacement perpendicular to freestream flow
- z = direction along cylinder axis, or fluid degree of freedom
- ρ = fluid mass density
- ζ_f = cylinder fluid damping factor, dimensionless
- ζ_n = cylinder damping factor, fraction of critical damping, dimensionless, in air with additional mass equal to fluid added mass in water
- ζ_o = cylinder damping factor, fraction of critical damping, dimensionless, in air, without magnetic damping or additional mass
- φ = phase angle between force and displacement (Eq. (4*b*))
- ω = circular frequency, $2\pi f$ (rad/s)
- ω_s = circular shedding frequency from stationary cylinder, $2\pi f$ (rad/s)
- ν = kinematic viscosity, 1.14×10^{-5} $\mathrm{ft^2/s}$ (0.01054 $\mathrm{cm^2/s}$) typical for experiment
- δ_r = reduced damping based on in-air damping factor; also, known as Scruton number, dimensionless, $2m(2\pi\zeta_n)/\rho D^2$

Appendix: Further Results

The equation of transverse motion of a uniform elastic cylinder responding to the two parameter lift force model (Eq. (15)) has a steady-state exact solution (Eq. (5)), if C_{mv} and C_{dv} are known.

$$\frac{A_y}{D}=\frac{1}{4\pi}\frac{\rho D^2}{2m(2\pi\zeta_n)}\left(\frac{U}{f_nD}\right)^2\{\zeta_nC_{mv}+\sqrt{\zeta_n^2C_{mv}^2+C_{dv}^2}\}$$

$$\frac{f}{f_n}=\frac{1}{C_{dv}}\{\zeta_nC_{mv}-\sqrt{C_{dv}^2+\zeta_n^2C_{mv}^2}\} \tag{A1}$$

The solution to Eq. (22*a*) for a given cylinder oscillation $y=A_y \sin \omega t$ is obtained by substituting $z=b_1 \cos \omega t+b_2 \cos \omega t$ into the equation, separating sine and cosine terms into two equations, setting $x=b_1\omega/A_{zo}\omega_s t$ and $y=b_1\omega/A_{zo}\omega_s$, $x^2+y^2=r^2$, and $\sigma=2\pi S(\omega_s^2-\omega^2)a_0/\omega\omega_s(a_1-a_{41})$ to produce a cubic in r^2 with an exact solution [67].

References

[1] Bearman, P. W., 1987, Private Communication.
[2] Jeon, D., and Gharib, M., 2004, "On the Relationship Between the Vortex Formation Process and Cylinder Wake Vortex Patterns," J. Fluid Mech., **519**, pp. 161–181.
[3] Khalak, A., and Williamson, C. H. K., 1999, "Motions, Forces and Mode Transitions in Vortex-Induced Vibrations at Low Mass-Damping," J. Fluids Struct., **13**, pp. 813–851.
[4] Dahl, J. M., Hover, F. S., and Triantafyllou, M. S., 2006, "Two Degree-of-Freedom Vortex-Induced Vibrations Using a Force Assisted Apparatus," J. Fluids Struct., **22**, pp. 807–818.
[5] Gabbai, R. D., and Benaroya, H., 2005, "An Overview of Modeling and Experiments of Vortex-Induced Vibration," J. Sound Vib., **282**, pp. 575–616.
[6] Govardhan, R. N., and Williamson, C. H. K., 2006, "Defining the Modified Griffin Plot in Vortex Induced Vibration," J. Fluid Mech., **561**, pp. 147–180.
[7] Norberg, C., 2003, "Fluctuating Lift on a Circular Cylinder: Review and New Measurements," J. Fluids Struct., **17**, pp. 57–96.
[8] Sarpkaya, T., 1995, "Hydrodynamic Damping, Flow-Induced Oscillations, and Biharmonic Response," ASME J. Offshore Mech. Arct. Eng., **117**, pp. 232–238.
[9] Pantazopoulos, M., 1994, "Vortex-Induced Vibration Parameters: Critical Review," ASME 13th International Conference on Offshore Mechanics and Arctic Engineering, Vol. 1, pp. 199–255.
[10] Blevins, R. D., 1990, *Flow-Induced Vibration*, 2nd ed., Krieger, Malabar, FL.
[11] Bearman, P. W., 1984, "Vortex Shedding From Oscillating Bluff Bodies," Annu. Rev. Fluid Mech., **16**, pp. 195–222.
[12] Achenbach, E., and Heinecke, E., 1981, "On Vortex Shedding From Smooth and Rough Cylinders in the Range of Reynolds Numbers 6×10^3 to 5×10^6," J. Fluid Mech., **109**, pp. 239–251.
[13] Norberg, C., 1987, "Reynolds Number and Freestream Turbulence Effect on the Flow and Fluid Forces of a Circular Cylinder in Cross Flow," Ph.D. thesis, Chalmers University of Technology, Goteborg, Sweden.
[14] Shih, W. C. L., Wang, C., Coles, D., and Roshko, A., 1993, "Experiments on Flow Past Rough Circular Cylinders at Large Reynolds Numbers," J. Wind Eng. Ind. Aerodyn., **49**, pp. 351–368.
[15] Tritton, D. J., 1959, "Experiments on the Flow Past a Circular Cylinder at Low Reynolds Numbers," J. Fluid Mech., **6**, pp. 547–567.
[16] Wieselsberger, V. C., 1921, "Neuere Feststellungen uber die Gesetze des Flussigkeits- und Luftwiderstandes," Phys. Z., **22**(11), pp. 321–328.
[17] Jones, G. W., Cincotta, J. J., and Walker, R. W., 1969, "Aerodynamic Forces on a Stationary and Oscillating Circular Cylinder at High Reynolds Numbers," National Aeronautics and Space Administration, Report No. NASA TR R-300.
[18] Allen, D., and Henning, D. L., 2001, "Surface Roughness Effects on Vortex-

Induced Vibration at Critical and Supercritical Reynolds Numbers," Offshore Technology Conference, Paper No. OTC 13302.
[19] Blevins, R. D., and Coughran, C. S., 2009, "Experimental Investigation of Vortex-Induced Vibration in One and Two Dimensions With Variable Mass, Damping, and Reynolds Number," ASME J. Fluids Eng., **131**, p. 101202.
[20] Anagnostoulos, P., and Bearman, P. W., 1992, "Response Characteristics of a Vortex Excited Cylinder at Low Reynolds Numbers," J. Fluids Struct., **6**, pp. 39–50.
[21] Zan, S. J., and Matsuda, K., 2002, "Steady and Unsteady Loading on a Roughened Circular Cylinder at Reynolds Numbers up to 900,000," J. Wind. Eng. Ind. Aerodyn., **90**, pp. 567–581.
[22] Roshko, A., 1954, "On the Drag and Shedding Frequency of Two-Dimensional Bluff Bodies," National Advisory Committee for Aeronautics, NACA Technical Note 3169.
[23] Fey, U., Kong, M., and Eckelmann, H., 1998, "A New Strouhal-Reynolds Number Relationship," Phys. Fluids, **10**(7), pp. 1547–1549.
[24] Toebes, G. H., 1969, "The Unsteady Flow and Wake Near an Oscillating Cylinder," ASME J. Basic Eng., **91**, pp. 493–502.
[25] Griffin, O. M., and Ramberg, S. E., 1974, "The Vortex Street Wakes of Vibrating Cylinders," J. Fluid Mech., **66**, pp. 553–576.
[26] Williamson, C. H. K., and Roshko, A., 1988, "Vortex Formation in the Wake of an Oscillating Cylinder," J. Fluids Struct., **2**, pp. 355–381.
[27] Zdravkovich, M. M., 1996, "Different Modes of Vortex Shedding: An Overview," J. Fluids Struct., **10**, pp. 427–437.
[28] Hartlen, R. T., and Currie, I. G., 1970, "Lift Oscillator Model of Vortex-Induced Vibration," J. Eng. Mech. Div., **96**, pp. 577–591.
[29] Sarpkaya, T., 1978, "Fluid Forces on Oscillating Cylinders," J. Wtrwy., Port, Coast., and Oc. Div., **104**, pp. 270–290.
[30] Mercier, J. A., 1973, "Large Amplitude Oscillations of a Circular Cylinder in a Low-Speed Stream," Ph.D. thesis, Stevens Institute of Technology.
[31] Staubli, T., 1983, "Calculation of the Vibration of an Elastically Mounted Cylinder Using Experimental Data From Forced Oscillation," ASME J. Fluids Eng., **105**, pp. 225–229.
[32] Moe, G., and Wu, Z.-J., 1990, "The Lift Force on a Circular Cylinder Vibrating in a Current," ASME J. Offshore Mech. Arct. Eng., **112**, pp. 297–303.
[33] Gopalkrishnan, R., 1993, "Vortex-Induced Forces on Oscillating Bluff Cylinders," Ph.D. thesis, Department of Ocean Engineering, MIT.
[34] de Wilde, J., et al., 2004, "Cross Section VIV Model Test for Novel Riser Geometries," DOT Conference, New Orleans, LA, Paper No. 12-3.
[35] Blackburn, H. M., and Melbourne, W. H., 1997, "Section Lift Force for an Oscillating Circular Cylinder," J. Fluids Struct., **11**, pp. 413–431.
[36] Morse, T. L., and Williamson, C. H. K., 2006, "Employing Controlled Vibrations to Predict Fluid Forces," J. Fluids Struct., **22**, pp. 877–884.
[37] Dahl, J. M., Hover, F. S., and Triantafyllou, M. S., 2008, "Higher Harmonic Forces and Predicted Vibrations From Forced Cylinder Motions," Proceeding of the 18th Offshore and Polar Engineering Conference, Vancouver, Canada.
[38] Blevins, R. D., and Burton, T. E., 1976, "Fluid Forces Induced by Vortex Shedding," ASME J. Fluids Eng., **95**, pp. 19–24.
[39] Thomson, W. T., 1988, *Theory of Vibration With Applications*, 3rd ed., Prentice-Hall, Englewood Cliffs, NJ.
[40] Bearman, P. W., Downie, M. J., Graham, J. M. R., and Obasju, E. D., 1985, "Forces on Cylinders in Viscous Oscillatory Flow at Low Keulegan–Carpenter Numbers," J. Fluid Mech., **154**, pp. 337–356.
[41] Sarpkaya, T., 1986, "Force on a Circular Cylinder in Viscous Oscillatory Flow at Low Keulegan–Carpenter Numbers," J. Fluid Mech., **165**, pp. 61–71.
[42] Chaplin, J. R., and Subbiah, K., 1998, "Hydrodynamic Damping of a Cylinder in Still Water and in Transverse Current," Appl. Ocean Res., **20**, pp. 251–259.
[43] Chaplin, J. R., 2000, "Hydrodynamic Damping of at Cylinder at $\beta \approx 10^6$," J. Fluids Struct., **14**, pp. 1101–1172.
[44] Skop, R. A., Ramberg, S. E., and Ferer, K. M., 1976, "Added Mass and Damping Forces on Circular Cylinders," Naval Research Laboratory, Report No. 7970.
[45] Otter, A., 1990, "Damping Forces on a Cylinder Oscillating in a Viscous Fluid," Appl. Ocean Res., **12**, pp. 153–155.
[46] Anaturk, A. R., Tromans, P. S., van Haxzendonk, H. C., Sluis, C. M., and Otter, A., 1992, "Drag Force on Cylinders Oscillating at Small Amplitude: A New Model," ASME J. Offshore Mech. Arct. Eng., **114**, pp. 91–104.
[47] Brouwers, J. J. H., and Meijssen, T. E. M., 1985, "Viscous Damping Forces on Oscillating Cylinders," Appl. Ocean Res., **7**, pp. 118–123.
[48] Honji, H., 1981, "Streaked Flow Around an Oscillating Circular Cylinder," J. Fluid Mech., **107**, pp. 509–520.
[49] Vandiver, J. K., 1993, "Dimensionless Parameters Important to the Prediction of Vortex-Induced Vibration of Long Flexible Cylinders in Ocean Currents," J. Fluids Struct., **7**, pp. 423–455.
[50] Wu, Z.-J., 1989, "Current Induced Vibrations of a Flexible Cylinder," Ph.D. thesis, Norwegian Institute of Technology, Trondheim.
[51] Toerum, A., and Anand, N. M., 1985, "Free Span Vibrations of Submarine Pipelines in Steady Flows—Effect of Free-Stream Turbulence on Mean Drag Coefficients," ASME J. Energy Resour. Technol., **107**, pp. 415–420.
[52] Szepessy, S., 1994, "On the Spanwise Correlation of Vortex Shedding From a Circular Cylinder," Phys. Fluids, **6**, pp. 2406–2416.
[53] West, G. S., and Apelt, C. J., 1997, "Fluctuating Lift and Drag Forces on Finite Lengths of a Circular Cylinder in the Subcritical Reynolds Number Range," J. Fluids Struct., **11**, pp. 135–158.
[54] Zdravkovich, M. M., 1982, "Scruton Number: A Proposal," J. Wind Eng. Ind. Aerodyn., **10**(3), pp. 263–265.
[55] Scruton, C., 1963, "On the Wind Excited Oscillation of Stacks, Towers, and Masts," Proceedings of the Conference on Wind Effects on Buildings and Structures, National Physical Laboratory, Teddington, England.
[56] Skop, R. A., and Balasubramanian, S., 1997, "A New Twist on an Old Model for Vortex-Excited Vibrations," J. Fluids Struct., **11**, pp. 395–412.
[57] Griffin, O. M., Skop, R. A., and Koopman, G. H., 1973, "The Vortex-Excited Resonant Vibrations of Circular Cylinders," J. Sound Vib., **31**, pp. 235–249.
[58] Sarpkaya, T., 2004, "A Critical Review of the Intrinsic Nature of Vortex Induced Vibrations," J. Fluids Struct., **19**, pp. 389–447.
[59] Feng, C. C., 1968, "The Measurement of Vortex-Induced Effects in Flow Past Stationary and Oscillating Circular and D-Section Cylinders," M.A.Sc. thesis, University of British Columbia.
[60] Facchinetti, M. L., de Langre, E., and Biolley, F., 2004, "Coupling of Structure and Wake Oscillators in Vortex-Induced Vibrations," J. Fluids Struct., **19**, pp. 123–140.
[61] Iwan, W. D., 1975, "The Vortex Induced Oscillation of Elastic Structural Elements," ASME J. Eng. Ind., **97**, pp. 1378–1382.
[62] Violette, R., de Langre, E., and Szydlowski, J., 2007, "Computation of Vortex-Induced Vibration of Long Structures Using a Wake Oscillator Model," Comput. Struct., **85**, pp. 1134–1144.
[63] Poore, A. B., Doedel, E. J., and Cermak, J. E., 1986, "Dynamics of the Iwan–Blevins Wake Oscillator Model," Int. J. Non-Linear Mech., **21**, pp. 291–302.
[64] Hall, S. A., and Iwan, W. D., 1984, "Oscillations of a Self-Excited Nonlinear System," ASME J. Appl. Mech., **97**, pp. 1378–1382.
[65] Hamid, E., 2009 "Semi-Empirical Time Doman VIV—Analysis Modle Based on Force Decomposition," M.S. thesis, Newcastle University, Newcastle.
[66] Meirovitch, L., 1967, *Analytical Methods in Vibrations*, Macmillan, NY, p. 235.
[67] Retorys, K., 1969, *Survey of Applicable Mathematics*, MIT, Cambridge, pp. 77–79.